Cystic Adenomatoid Malformations Are Induced by Localized FGF10 Overexpression in Fetal Rat Lung

Sílvia Gonzaga[1,2*], Tiago Henriques-Coelho[1,3*], Marcus Davey[1], Philip W. Zoltick[1], Adelino F. Leite-Moreira[3], Jorge Correia-Pinto[2], and Alan W. Flake[1]

[1]The Children's Center for Fetal Research, Children's Hospital of Philadelphia, Philadelphia, Pennsylvania; [2]Life and Health Sciences Research Institute (ICVS), School of Health Sciences, University of Minho, Braga, Portugal; and [3]Department of Physiology, Oporto Medical School, University of Porto, Porto, Portugal

Fibroblast growth factor-10 (FGF10) is a mesenchymal growth factor, involved in epithelial and mesenchymal interactions during lung branching morphogenesis. In the present work, FGF10 overexpression was transiently induced in a temporally and spatially restricted manner, during the pseudoglandular or canalicular stages of rat lung development, by trans-uterine ultrasound-guided intraparenchymal microinjections of adenoviral vector encoding the *rfgf10* transgene. The morphologic and histologic classification of the resulting malformations were dependent upon developmental stage and location. Overexpression of FGF10 restricted to the proximal tracheobronchial tree during the pseudoglandular phase resulted in large cysts lined by tall columnar epithelium composed primarily of Clara cells with a paucity of Type II pneumocytes, resembling bronchiolar type epithelium. In contrast, FGF10 overexpression in the distal lung parenchyma during the canalicular phase resulted in small cysts lined by cuboidal epithelial cells composed of primarily Type II pneumocytes resembling acinar epithelial differentiation. The cystic malformations induced by FGF10 overexpression appear to closely recapitulate the morphology and histology of the spectrum of human congenital cystic adenomatoid malformation (CCAM). These findings support a role for FGF10 in the induction of human CCAM and provide further mechanistic insight into the role of FGF10 in normal and abnormal lung development.

Keywords: fibroblast growth factor-10; congenital cystic adenomatoid malformation; adenoviral vector; lung development; gene transfer

CLINICAL RELEVANCE

Our results demonstrate that overexpression of a single gene induces cystic lung lesions resembling the entire spectrum of congenital cystic adenomatoid malformation (CCAM). These results provide unique insight into developmental mechanisms that may contribute to CCAM formation.

Fibroblast growth factors (FGFs) comprise a family of potent mitogens that regulate cellular proliferation, migration, and differentiation (1, 2). Two members of the FGF family, FGF7 and FGF10, are expressed in lung mesenchymal cells in distinct spatial and temporal patterns. FGF7 expression begins at Embryonic Day (E)14.5 and is expressed throughout the mesenchyme surrounding the developing lung tubules (3, 4). FGF10 expression is initiated earlier at the onset of lung organogenesis and is restricted to the mesenchyme surrounding the distal tips of the branching tubules (5). Both FGF7 and FGF10 bind with high affinity to the same FGF receptor isoform, FGFR2b (6, 7). FGFR2 expression is restricted to the epithelial cells of the developing lung at the onset of lung organogenesis at E9.5, and moves more peripherally in epithelial distribution with ongoing lung development (7). These distinct patterns of expression of FGF7 and FGF10 in lung mesenchyme and the simultaneous expression of FGFR2 in respiratory epithelial cells implicate a primary role for FGF mesenchymal/epithelial signaling in lung morphogenesis. The control of the bud size and shape during branching is achieved by an intricate exchange of signals between the growing bud and the surrounding mesenchyme. As the bud elongates, FGF10/FGFR2 signaling induces expression of Spry2 and Bmp4 in the distal epithelium. Spry2 is one of the earliest factors to be induced and limits the proliferation of the lung epithelium (8, 9). Bmp4 disrupts distal budding when expression is activated via an autocrine mechanism (10, 11).

Much of what is currently known about the role of the FGFs and other individual mediators of lung morphogenesis has been derived from analysis of phenotypes induced by either targeted disruption, or ectopic transgenic overexpression of the candidate genes. Targeted disruption of *fgf10* results in absence of lung structures distal to the mainstem bronchi, and this phenotype is replicated in *fgfr2b* knockout mice, confirming a critical role for this signaling pathway in lung development (12, 13). In contrast, mice with targeted disruption of *fgf7* have normal lungs (14), indicating that this polypeptide is not required for normal lung morphogenesis or that the FGF peptides have redundant functions. Ectopic overexpression of either factor in respiratory epithelium using epithelium specific promoter genes results in marked perturbations of lung morphogenesis. FGF7 overexpression is uniformly lethal by E16, inducing massive cysts of the pulmonary parenchyma reminiscent of the macrocystic form of cystic adenomatoid malformation (15). Conditional ectopic overexpression of FGF10 in the respiratory epithelium at later stages of gestation markedly perturbs lung morphogenesis and causes dense, adenomatous malformations (16). These effects appear to be mediated by the proliferative and chemoattractant effects of FGFs on lung epithelium. FGF7 has potent mitogenic effects on pulmonary epithelial cells inducing proliferation of bronchial epithelial and mature type II alveolar cells (4, 17). FGF10 acts as a mitogen and chemoattractant, inducing directional growth of the lung buds in close proximity (5, 18, 19) during the earliest stages of lung development. While the above studies are elucidating in many

(*Received in original form July 29, 2007 and in final form February 23, 2008*)

*These authors contributed equally to this manuscript.

This project was in part funded by proceeds from the Ruth and Tristram C. Colket Jr. Chair in Pediatric Surgery (A.W.F.), and the Fundação para a Ciência e Tecnologia (POCI/SAUOBS/56428/2004). S.G. was supported by FCT grant ref. SFRH/BD/15260/2004.

Correspondence and requests for reprints should be addressed to Alan W. Flake, M.D., Department of Surgery, The Children's Hospital of Philadelphia, Abramson Research Center, Rm 1116B, 3615 Civic Center Blvd., Philadelphia, PA 19104-4318. E-mail: flake@email.chop.edu

Am J Respir Cell Mol Biol Vol 39. pp 346–355, 2008
Originally Published in Press as DOI: 10.1165/rcmb.2007-0290OC on April 17, 2008
Internet address: www.atsjournals.org

ways, they also emphasize that the effects of specific lung growth factors on normal or abnormal lung development are highly dependent upon timing, duration, and distribution of expression. Global, ectopic expression of these highly spatially and temporally restricted growth factors may induce artifactual effects not seen with more compartment-appropriate overexpression, including autocrine effects and absence of normal directional induction. We reasoned that a more physiologic and discrete approach to dissection of FGF10 effects on lung development would be to induce transient, mesenchymal, overexpression in a localized area of the developing lung during specific stages of lung development.

We recently described an efficient method for gene transfer to fetal lung interstitial cells during the pseudoglandular stage of lung development by direct ultrasound-guided intrapulmonary injection of viral vectors (20). Furthermore, we demonstrated that adenoviral vector induced a rapid onset but relatively transient expression of the reporter gene relative to lentiviral vector. It occurred to us that this model might be valuable for investigation of the effects of transient and localized mesenchymal overexpression of specific growth factors on lung development.

In the present work, we hypothesized that focal FGF10 mesenchymal overexpression during lung development would cause focal abnormalities of epithelial proliferation. To test this hypothesis, we injected a bi-cistronic adenoviral vector encoding the *rfgf10* and *egfp* transgenes (AdGFP-FGF10) into targeted areas of fetal rat lung parenchyma, at specific stages of lung development. We observed that FGF10 overexpression resulted in the induction of consistent patterns of malformation, the appearance of which were developmental stage and location dependent. These malformations, in total, appear to closely recapitulate the morphology and histology of the entire spectrum of human congenital cystic adenomatoid malformation (CCAM).

MATERIALS AND METHODS

All experimental protocols were approved by the Institutional Animal Care and Use Committee at the Children's Hospital of Philadelphia and followed guidelines set forth in the National Institutes of Health Guide for the Care and Use of Laboratory Animals.

Viral Vector Preparation

Cell culture. 293 cells were kindly provided by the Gene Therapy Program (Division of Medical Genetics, University of Pennsylvania, Philadelphia, PA). Cells were grown in Dulbecco's modified Eagle's medium (DMEM) (Life Technologies/Invitrogen, Carlsbad, CA) supplemented with 10% fetal bovine serum (FBS) (Hyclone, Logan, UT), 100 units/ml penicillin, and 100 μg/ml streptomycin (Life Technologies/Invitrogen) at 37°C in a 5% CO_2 humidified atmosphere.

Rat FGF10 cds and recombinant adenovirus constructions. A cDNA library was prepared from newborn Sprague-Dawley lung using Trizol Reagent and Superscript (Invitrogen, Carlsbad, CA) as per manufacturers' recommendations. The rat *FGF10* cds was amplified using the forward primer 5′-gcggccgcc atgtggaaatggatactgacacattg-3′ and reverse primer 5′-ctcgaggctagcctatgagtggaccaccatg-3′ using standard methods and confirmed by sequence analysis (GenBank Sequence Database accession number NM_012951). The first-generation recombinant human adenovirus serotype 5 vector expressing the rat *FGF10* cds was synthesized as previously reported (21) with the following modifications. The rat *FGF10* cds was subcloned into a previously modified pShuttle-CMV vector containing a multiple cloning site and IRES-GFP cassette downstream to the promoter. Approximately 1 μg of the *Pme*I linearized shuttle vector DNA was electroporated into *Escherichia coli* BJ5183 harboring the pAdEasy-1 vector. Selected colonies were screened by restriction digests for the presence of size correct homologous recombined plasmids. The pAd-CMV-Rat FGF10-IRES-GFP plasmid DNA transformed the *recA–E. Coli*, DH10B, by electroporation for large-scale amplification. Five micrograms of *Pac*I-linearized pAd-CMV-Rat FGF10-IRES-GFP DNA was combined with Maxfect (Mediatech, Herndon, VA) as per manufacturer's instructions and used to transfect 293 cells. Transfected cells were monitored for GFP expression and cytopathic effect. Twelve days later, cells and cell debris were removed, pelleted, and after three cycles of freeze/thawing a viral lysate was obtained, identified as Ad-ratFGF10. To assure the production of rat FGF10 protein, 293 cells were infected with the viral lysate, and 48 hours later growth media was assayed for the presence of rat FGF10 by Western blot using a rabbit anti-Rat FGF10 antibody (H-121:sc-7919; Santa Cruz Biotechnology, Santa Cruz, CA) at 1/200 dilution. Propagation, concentration, and purification of the Ad-ratFGF10 was performed using Vivapure AdenoPACK 500 kit (Sartorius, Edgewood, NY) following manufacturer's recommendations. The viral pellet was resuspended in storage buffer (20 mM Tris-HCl, 25 mM NaCl, 2.5% glycerol, pH = 8) and stored at −80°C. Titer was determined in triplicate using serial dilutions of viral stock on 293 cells. Two days later, titers were determined by counting the number of GFP-positive colonies/field.

Ultrasound-Guided Injections

Time-dated pregnant Sprague-Dawley (Charles-River, Boston, MA) rats at 15.5 (E15.5; $n = 42$) and 18.5 (E18.5; $n = 18$) days *post-coitum* were anesthetized and a laparotomy was performed. Ultrasound-guided injections were performed as previously described (20). Briefly, fetuses were positioned to obtain axial views of the lungs in B-mode (VisualSonics, Toronto, Canada). The tip of the micropipette was brought into the image plane and was physically advanced through the uterine wall and amniotic cavity into the lung. A volume of 25 nl was injected using a remote control injector. After injections, dams were allowed to recover in a warming chamber. Two types of injections were performed with respect to the level of the bronchopulmonary tree. Injections performed near the main bronchus were defined as proximal. Injections performed at the peripheral basal area of the lung were defined as distal.

Ultrasound and Magnetic Resonance Imaging

Fetuses to be analyzed at E16.5, E18.5, and E21.5 were first inspected for lung morphology by ultrasound biomicroscopy. After performing laparotomy, the uterus was partially removed from the abdomen exposing one or two fetuses. Fetuses were covered with warmed sterile ultrasound gel and positioned to obtain axial views of the lungs in B-mode using a 40-MHz probe (VisualSonics).

Lung morphology of pups 1 week old (P7) was examined by magnetic resonance imaging using a Bruker Advance 400 wide-bore NMR spectrometer (Bruker AXS Inc., Madison, WI) equipped for microimaging. The Bruker self-shielded gradients were used with a 25-mm-diammeter RF coil to image the whole pups. After isoflurane overdose and neck dislocation, lungs were instilled intratracheally with perfluorocarbon to increase contrast and reduce susceptibility artifacts. Pups were inserted vertically into an 18-mm glass tube filled with Fomblin (perfluoropolyether), a liquid that approximately matches the susceptibility of tissue and does not give any background signal. Axial, coronal, and sagittal slices through the thoracic cavity were acquired with a spin echo T2 weighted pulse sequence, in which each image represents the sum of four echoes. For each orientation, 16 contiguous slices of 0.5 mm thickness were acquired with a square field of view (FOV) of 18 mm, a square matrix of 256 × 256 giving an in-plane resolution of 70 μm^2. The images were acquired using the following parameters: bandwith 50 kHz, pulse length 2 ms, repetition time 2 s, echo time 12 ms, and 2 excitations. Fetuses were screened inside the uterus at E16.5, E18.5, E19.5, and E21.5 dpc, and after being anesthetized, at 1 week (P7). The fetuses were positioned to get axial views of the lungs in B-mode and were screened in 3D-mode. After screening, fetuses and pups were harvested and lungs collected for stereomicroscopy, histology, and biochemical analysis.

Stereomicroscopy

Injected fetuses were visualized under a fluorescence stereomicroscope (MZ16FA; Leica, Heerburgg, Switzerland) immediately after harvesting, to evaluate enhanced green fluorescent protein expression, transduction efficiency, and biodistribution of the vector within lungs, trachea, heart, and diaphragm.

Histology and Immunohistochemistry

Specimens for histologic analysis were fixed in formalin (10%) and processed for paraffin sections. Immunostainings were performed on 4-μm-thick paraffin-embedded sections. After dewaxing in xylene and rehydration in ethanol, slides were blocked for specific serum (1:10 dilution) for 30 minutes at room temperature (RT) followed by incubation at 4°C with each primary antibody. The primary antibodies were monoclonal mouse EPOS anti–α-SMA (U.7033; Dako, Carpinteria, CA), polyclonal rabbit anti–Clara cell secretory protein (CCSP) (1:800 dilution; Seven Hills Bioreagents, Cincinnatti, OH), polyclonal rabbit anti-pro–surfactant protein (SP)-C (1:100 dilution; Chemicon, Temecula, CA), and polyclonal rabbit anti-GFP (1:100 dilution; Invitrogen). Samples were incubated with 3% hydrogen peroxide in methanol for 30 minutes at room temperature to quench endogenous peroxidase. Incubation with secondary antibody biotinylated goat anti-polyvalent (UltraVision HRP Detection System; Lab Vision, Fremont, CA) was performed at room temperature for 30 minutes. Slides were incubated with avidin–biotin complex (1:200 dilution; Vector Laboratories, Burlingame, CA) and developed with 3, 3′-diaminobenzidine (DAB) substrate kit (SK-4100; Vector Laboratories). Sections were counterstained with Harris hematoxylin. The sections were visualized under the Olympus BX61 microscope and photographed using an Olympus DP70 camera (Olympus America, Center Valley, PA). Adjacent sections were also stained with hematoxylin and eosin for morphologic studies.

In Situ Hybridization

Digoxigenin-labeled rat FGF10 antisense and sense probes were produced from the 648-bp sequence cloned in pIBI31, linearized using *NheI* or *NotI*, and transcribed with T3 or T7 polymerases, respectively. The following mouse cDNAs were used to generate digoxigenin-labeled riboprobes: 1.0 kb *Bmp4* and 948 bp *Spry2* (kindly provided by Dr. Saverio Bellusci). Lungs were fixed overnight at 4°C in 4% formaldehyde-2 mM EGTA, rinsed in PBS, dehydrated through a methanol series, and stored in 100% methanol at −20°C. Whole-mount (FGF10) and tissue section (BMP4 and Spry2) *in situ* hybridization were performed according to procedures described previously (22, 23). Lungs were visualized as whole mounts in PBT (PBS, 0.1% Tween20) under a dissecting microscope stereomicroscope and photographed with an Olympus 2100 camera. Whole mount lungs were embedded in 2-hydroxyethyl methacrylate (Technovit 7100; Heraeus Kulzer GmbH, Hanau, Germany) and processed for sectioning at 15 μm thickness using a rotary microtome (Leica RM 2155). Hybridized lungs sections were photographed using an Olympus DP70 camera coupled to an Olympus BX61 microscope.

Quantitative PCR

Samples from injected lungs collected at E16.5, E18.5, and E21.5 were placed in 1.5 ml microcentrifuge tubes, immediately frozen in liquid nitrogen, and stored at −80°C.

To examine rFGF-10 gene expression, total RNA from each lung specimen was isolated using TRIzol Reagent (Invitrogen, Carlsbad, CA), reverse transcribed, and subjected to quantitative polymerase chain reaction (qPCR) analysis as previously described (24–26). First-strand cDNA was prepared from 1 μg total cellular RNA isolated above. Total cDNA was used for the relative quantification by real time-PCR of rFGF10 and of the reference gene, rβ-actin, using the ABI PRISM 7700 s Sequence Detection System (Applied Biosystems, Foster City, CA). Sequence data were obtained from the GenBank Sequence Database (accession numbers: NM_031144, *Rattus norvegicus* rβ-actin; NM_012951, *R. norvegicus* FGF10 mRNA). Pre-designed TaqMan Gene Expression Assays were used for rFGF10 (Rn00564115_m1; Applied Biosystems), β-actin (Rn00667869_m1; Applied Biosystems). Amplification conditions were identical for all reactions. The thermal profile was as follows: 2 minutes at 50°C, 10 minutes of denaturation at 95°C, 40 cycles of denaturation at 95°C for 15 seconds, and annealing and extension at 60°C for 1 minute. The amplification reactions were set in a final volume of 20 μl, containing 1× TaqMan Universal PCR Mastermix (Applied Biosystems), 100 ng of the cDNA sample, 900 nM of each primer, and 250 nM of the respective probe. Negative control was included in all the runs, which consisted of omitting the cDNA and performing a melting curve analysis. β-actin, rFGF10, standard amplification curves (ST curve) were made with randomly selected cDNA samples (setting at r = 0.99). For each experimental group studied, three samples were analyzed, in triplicate, and mean result was used for further analysis. Amplification data were analyzed by the sequence detection system software (SDS 1.2 version; Applied Biosystems).

Statistical Analysis

The results were presented as mean ± SE. To ascertain the statistical significance of the differences in the levels of mRNA, one-way ANOVA was performed. Upon statistically significant differences, a Student-Newman-Keuls test was selected to perform pairwise multiple comparisons. Survival rates were compared by the log-rank test. Differences between groups were considered to be statistically significant when $P < 0.05$.

RESULTS

Intraparenchymal Injection of AdGFP-FGF10 during the Pseudoglandular Stage Results in Pulmonary Morbidity

We investigated the effects of localized FGF10 overexpression on fetal rat lungs during the pseudoglandular and canalicular stages of lung development by performing transuterine ultrasound-guided microinjections of AdGFP-FGF10 at E15.5 and E18.5 by our previously described technique. Pre- and postnatal imaging analysis revealed the presence of cystic lesions in the injected lungs without obvious other abnormalities. External morphology of injected fetuses among all the groups was normal, as was the macroscopic structure of diaphragm, heart, and thoracic cavity. At cesarean, we detected a prenatal mortality rate of 26% and 10% associated with lung injections at E15.5 and E18.5, respectively, with control PBS injections. This was comparable to our previous study (20) using the same methodology and comparing PBS with the identical AdGFP vector minus the FGF10 transgene. In that study, survival to cesarean section was 81 ± 6% and 87 ± 4% for PBS and AdGFP, respectively. It is also important to note that in that study, no pulmonary cystic changes were seen in any animals injected with PBS or AdGFP vector alone. When AdGFP-FGF10 was injected at E15.5, there was an additional mortality during the first hours of postnatal life that reduced the survival rate to 33% by the seventh day after birth. Some pups that were injected at E15.5 were cyanotic and displayed gasping respiratory efforts within a few hours after birth, with subsequent demise. Autopsies or magnetic resonance imaging (MRI) examination revealed very large cysts that occupied almost all of the ipsilateral hemithorax. In contrast, when AdGFP-FGF10 was injected at E18.5, the survival rate was not statistically different from that of PBS-injected controls and no macrocystic lesions were seen. Pups that survived until the seventh day after birth displayed overtly normal activity levels and appeared developmentally normal. There were no maternal deaths.

Phenotype of the Lung Cystic Malformation Is Developmental Stage Dependent

To assess the effect of focal FGF10 overexpression on lung development during critical periods of lung morphogenesis, we performed *in utero* gene transfer during the rat pseudoglandular (E15.5) and canalicular (E18.5) stages of lung development. Lungs were analyzed by ultrasound, MRI, gross appearance, and fluorescence stereomicroscopy at different pre and postnatal time points (Figure 1).

When FGF10 gene transfer was performed at E15.5, malformations containing large cysts were detected as early as 24 hours after injection (Figures 1a–1c). The malformations persisted during the remainder of gestation (Figures 1d–1i) and at

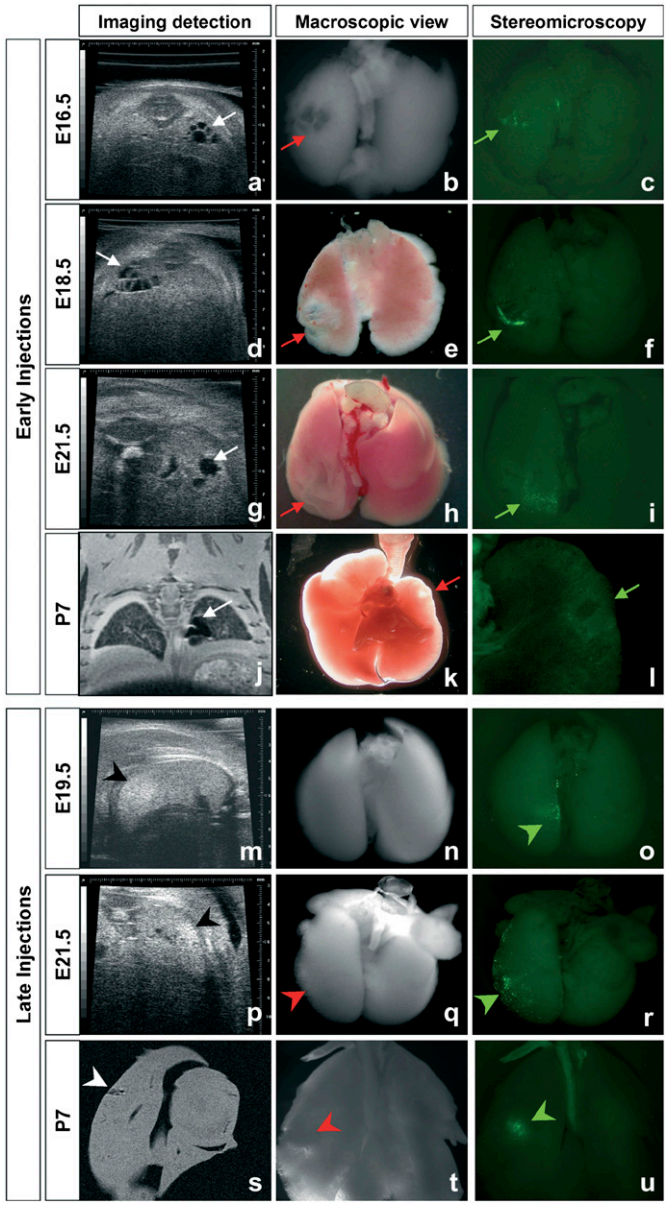

Figure 1. Developmental stage dependence of cystic malformations. Fetuses injected at Embryonic Day (E)15.5 were analyzed at E16.5, E18.5, E21.5, and Postnatal Day (P)7 (*a–l*). Representative images of injected lungs demonstrate macrocystic malformations (*white arrows*) by ultrasound at prenatal time points and magnetic resonance imaging (MRI) at P7. The macrocysts appeared within 24 hours after injection (*a–c*) and persisted until P7 (*j–l*) and were large enough to be easily appreciated by gross examination (*red arrows*). The expression of enhanced green fluorescent protein (EGFP) coincided with the affected area (*c, f, i, l, green arrows*). Fetuses injected at E18.5 were analyzed at E19.5, E21.5, and P7 (*m–u*). Microcystic malformations were detected by ultrasound at E19.5 (*m*) and E21.5 (*p*) as an area of increased echogenicity (*black arrowheads*) and were visualized as small cysts on MRI at P7 (*s, white arrowheads*). The malformations were present by E19.5 and persisted until P7, with the area of the malformation coinciding with the area of EGFP expression (*o, r, u, green arrowheads*).

1 week after birth (Figures 1j–1l). Imaging of these lesions revealed fluid-filled areas of low echogenicity with thin intervening septa surrounded by normal lung parenchyma. Gross inspection revealed lung malformations characterized by a single or usually multiple large cysts that were lined by a thin membrane. The cysts were always restricted to a single lobe of the lung. Analysis by fluorescence stereomicroscopy demonstrated that the affected area coincided with the area of gene transfer, as confirmed by GFP expression. At birth after ventilation of the neonatal lung, the cysts were immediately filled with air. The communication between the main airways and the cysts was confirmed by bronchofluoroscopy (data not shown).

In contrast, when FGF10 gene transfer was performed at E18.5, prenatal ultrasound imaging revealed hyperechogenicity in the area injected within 24 hours after injection, with only rare instances of visible cysts by ultrasound or gross inspection (Figures 1m–1r). These malformations were not easily detected by gross inspection; however, postnatal MRI revealed restricted areas with several small cysts (Figure 1s).

Phenotype of the Malformation Is Spatially Dependent

To explore the effect of FGF10 gene transfer at different levels of the bronchopulmonary tree, injections localized to either the proximal or the distal areas of the developing lung were analyzed at term (E21.5) (Figure 2). When the injections were performed at E15.5, proximal injections (Figures 2a–2c) induced larger cysts than distal injections (Figures 2d–2f), but the number of cysts were greater in the distal injection group. In contrast, injections into either the proximal or distal lung parenchyma at E18.5 induced only small cysts on microscopic analysis (Figures 2g–2l). Relative to the early injections, the affected area was more restricted and no macroscopic cysts were clearly seen. In all groups, lesions were well demarcated histologically from the adjacent normal lung parenchyma.

Histologic Characterization of Induced Cystic Lung Malformations

Specimens from lungs injected either at E15.5 or E18.5 were harvested at E21.5 and processed for histologic analysis and immunohistochemistry for α-smooth muscle actin (α-SMA), CCSP, SP-C, and green fluorescence protein (GFP) (Figure 3 and Table 1). Lungs injected at E15.5 targeting the proximal bronchopulmonary tree demonstrated one to four large predominant cysts surrounded by normal lung parenchyma (Figures 3f–3j). These cysts were lined by tall columnar pseudostratified epithelium encircled by a well-defined muscular wall composed of two to three cell layers. Most of the cells lining the cysts were positive for CCSP, whereas only a few cells stained for pro–SP-C, indicating a predominance of Clara cells and a paucity of Type II pneumocytes, respectively. Cartilage and skeletal muscle were absent. In lungs injected at E15.5 with gene transfer to the distal lung parenchyma, several large cysts appeared in the injected area which were lined with cuboidal to tall columnar epithelium (Figures 3k–3o). Smooth muscle fibers could be detected surrounding the cysts forming an incomplete layer. Within the cysts there was a sharp boundary between positive and negative areas for CCSP, corresponding to the transition between terminal and respiratory bronchioles. There was an intense staining for pro–SP-C in the epithelial lining of the cysts. Cystic malformations in fetuses injected at E15.5 were separated by thin septa with only a small amount of interstitial tissue.

Injections targeting the proximal lung parenchyma at E18.5 resulted in multiple relatively small-size cysts compared with the early injection time point (Figures 3p–3t). These cysts were lined by cuboidal epithelium with few Clara cells and rare type II pneumocytes. Smooth muscle fibers could be detected surrounding the cysts forming an incomplete layer. Injections targeting the distal lung parenchyma at E18.5 resulted in several types of small cysts (Figures 3u–3y). Some resembled bronchioles, while others contained intricate folds. The lining

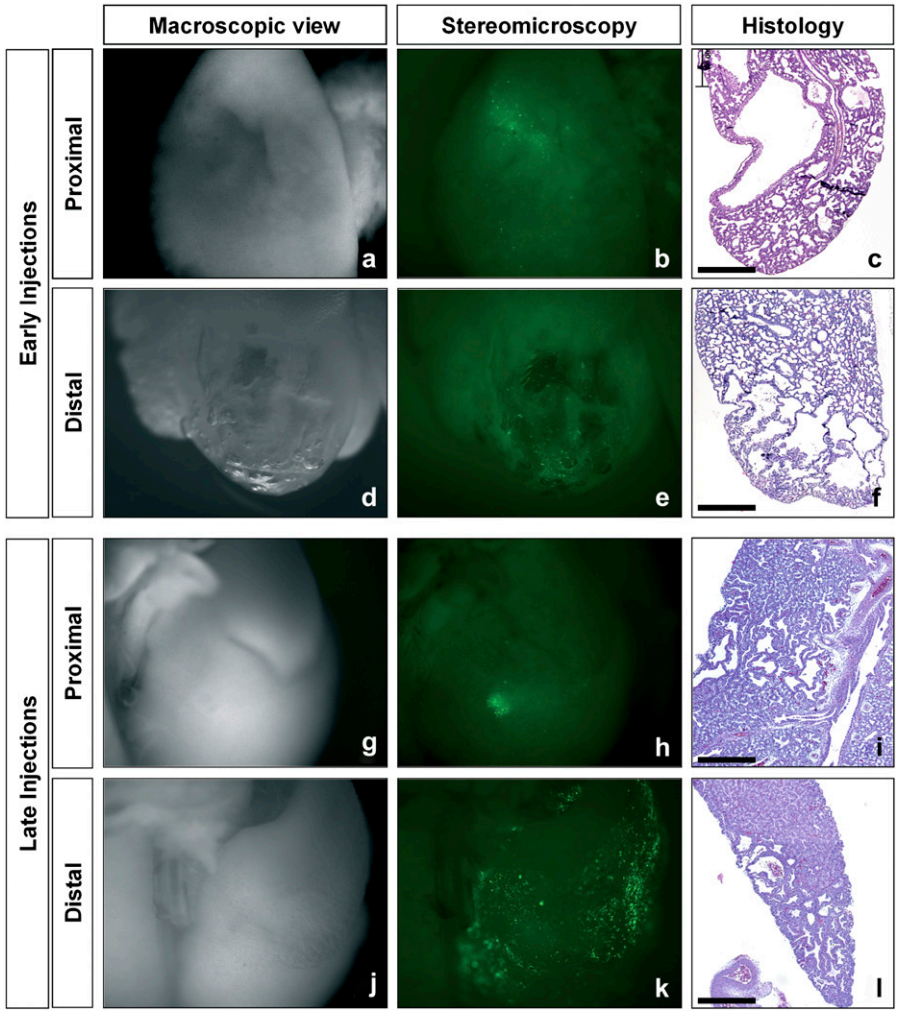

Figure 2. Spatial dependence of cystic malformations. Fetal injections of viral vector targeted proximal versus distal areas of the pulmonary tree and lungs were analyzed at E21.5. Early proximal injections of AdGFP-FGF10 (*a–c*) induced the formation of a few large cysts within the central lung parenchyma easily detectable by macroscopic inspection. Early distal injections of AdGFP-FGF10 (*d–f*) induced the formation of several large cysts visible in the periphery of the lung, but the cysts were smaller than with proximal injections. Late FGF10 gene transfer (*g–l*) induced the formation of small cysts that were barely macroscopically detectable. Once again, the cysts were larger with proximal injections (*g-i*) than distal injections (*j–l*). The overall affected area in late injections was more restricted than that inearly injections. In all groups, GFP expression (*b, e, h, k*) coincided with the location of the cysts and the malformations were well demarcated from the adjacent normal lung parenchyma. *Scale bars* correspond to 500 μm.

epithelium was composed primarily of type II pneumocytes. Clara cells were absent. Expression of α-SMA revealed the presence of scattered smooth muscle cells. Relative to the E15.5 injected group, fetuses injected at E18.5 displayed septa between the cysts that contained a moderate to abundant amount of loose mesenchymal-type interstitium. As we noted in our previous study (20) the distribution of gene transfer as confirmed by GFP immunohistochemistry (Figures 3j, 3o, 3t, 3y) appeared to be restricted to the mesenchyme in all lungs injected with AdGFP-FGF10.

Location and Quantification of Lung FGF10 Overexpression

FGF10 mRNA expression was detected by whole mount *in situ* hybridization (wISH) 24 hours after injections in both the early and late injected groups (Figures 4a–4o). The normal pattern of FGF10 expression observed in the PBS-injected control lungs was profoundly altered by FGF10 gene transfer. In all injected lungs examined, an increase in FGF10 mRNA expression was observed in an area that corresponded to the area of expression of GFP. On tissue sections of hybridized lungs, FGF10 overexpression in both early and late injected lungs appeared to be restricted to the mesenchymal compartment of lung parenchyma (Figures 4j and 4o), in agreement with the GFP immunohistochemistry.

Quantification of *FGF10* mRNA levels was performed at E16.5, E18.5, and E21.5 in ipsilateral and contralateral lungs injected at E15.5 and compared with PBS-injected control lungs (Figure 4p). *FGF10* mRNA expression was significantly increased in only the injected lung at 24 hours after injection. Levels of *fgf10* mRNA in injected lungs returned to levels measured in PBS control groups at E18.5 and E21.5.

Expression Pattern of BMP4 and Spry2 in Cystic Malformations

The expression pattern of *BMP4* and *Spry2* was characterized by *in situ* hybridization (ISH) 24 hours after injection in both early and late injected lungs (Figure 5). For early injected lungs, aside from the cystic morphology, the pattern of expression of BMP4 and Spry2 did not seem significantly altered in comparison with the PBS controls (Figures 5a–5d). In contrast, for late injected lungs expression of BMP4 and Spry2 appears significantly increased relative to controls in the epithelium of the cystic malformations (Figures 5e–5h).

DISCUSSION

FGF10 overexpression from the mesenchyme was focally and transiently induced at different locations and developmental stages in the fetal rat lung using our method of intraparenchymal gene transfer. In the area of forced FGF10 expression, pulmonary morphogenesis was markedly perturbed with the very rapid appearance of localized cystic lung malformations. The type of malformation observed was developmental stage and location dependent, with the spectrum ranging from macrocystic

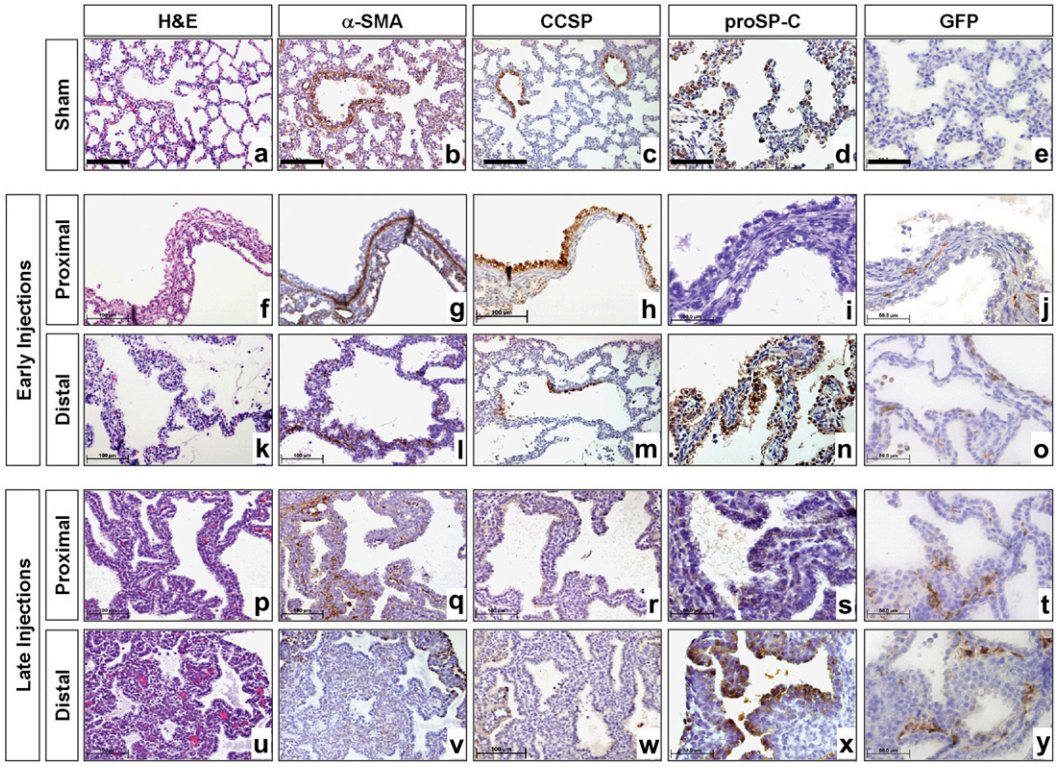

Figure 3. Histologic characterization of cystic malformations. Specimens from fetuses injected in the proximal and distal lung parenchyma at E15.5 (*f–o*) and E18.5 (*p–y*) were analyzed at E21.5. Lungs injected at E15.5 targeting the proximal area of bronchopulmonary tree presented large cysts encircled by a well-defined muscular wall composed of two to three cell layers (*g*). Cysts were lined by tall columnar pseudostratified epithelium (*f*) and the majority of the cells lining the cysts were positive for CCSP (*h*), with very few cells expressing proSP-C (*i*). In contrast, lungs injected into the distal parenchyma at E15.5 demonstrated several large cysts that were lined with cuboidal to tall columnar epithelium (*k*). Subepithelial smooth muscle fibers could be detected forming an incomplete layer (*l*). Cystic epithelium was predominantly positive for pro–surfactant protein (SP)-C (*n*), whereas CCSP immunostaining revealed a sharp boundary between positive and negative areas (*m*). Cystic malformations in fetuses injected at E15.5 were separated by thin septae containing a small amount of interstitial tissue. Injections at E18.5 resulted in relatively small cysts lined by cuboidal epithelium and separated by a moderate to abundant amount of loose mesenchymal type of interstitium (*p*, *u*). Cystic malformations caused by proximal injections contained few CCSP-positive cells (*r*), rare proSP-C-positive cells (*s*) and an incomplete subepithelial smooth muscle layer (*q*). Cystic malformations secondary to distal injections were lined by proSP-C positive cells (*x*) and scattered smooth muscle cells were present (*v*). In all groups, GFP positive cells were restricted to the interstitial compartment of lung parenchyma (*j*, *o*, *t*, *y*). In all groups cartilage and skeletal muscle were absent. *Scale bars* correspond to 100 μm for hematoxylin and eosin, α-smooth muscle actin, and CCSP and 50 μm for pro–SP-C and GFP immunostaining.

malformations lined by predominantly bronchial epithelium, to microcystic malformations lined by predominantly alveolar epithelium. The malformations were detectable by prenatal ultrasound examination within 24 hours after vector injection, and persisted until at least 1 week after birth. Whether examined grossly, by pre or postnatal imaging, or microscopically, the malformations appeared remarkably similar to the spectrum of human malformations characterized as congenital cystic adenomatoid malformation (CCAM).

The present study differs from previous studies examining the effect of FGF10 overexpression during lung development in several important ways. Expression of FGF10 in this study was

TABLE 1. HISTOLOGIC CHARACTERIZATION OF CYSTIC MALFORMATIONS

	E15.5 Proximal	E15.5 Distal	E18.5 Proximal	E18.5 Distal
Cyst size	Large	Large	Small	Small
Number of cysts	Few	Several	Few	Several
Epithelial lining	Tall columnar pseudo-stratified	Cuboidal to tall columnar	Cuboidal	Cuboidal
α-SMA	Well-defined muscular layer	Discontinuous bands of smooth mucle	Discontinuous bands of smooth mucle	Scattered expression
CCSP	+++	+	+/−	—
SP-C	+/−	+++	—	+++

Definition of abbreviations: α-SMA, α-smooth muscle actin; CCSP, Clara cell secretory protein; E, Embryonic Day; SP-C, surfactant protein C.

focal rather than diffuse, and was expressed in interstitial cells rather than ectopically from respiratory epithelium. In our previous study (20) assessing the distribution of marker gene expression after intraparenchymal injection, we demonstrated that gene expression could be limited to a small area of lung parenchyma by limiting the volume of injection, and that expression was confined to the interstitial compartment of the lung with no demonstrable co-localization with SP-B–expressing epithelial cells. This distribution of expression was confirmed in this study by both GFP immunohistochemistry and wISH for FGF10. Another important difference is that the expression in this study was relatively transient. This was due to the use of adenoviral vector allowing rapid onset of expression with peak expression occurring approximately 24 hours after injection. The expression profile of FGF10 documented in this study is in good agreement with our previous study (20) in which quantitative PCR was used to assess GFP mRNA expression using the AdGFP control vector. The rapid diminution of transgene expression in both studies is consistent with the known episomal location of adenoviral gene expression, the small volume of vector administered (25 nl), and the rapid proliferation of fetal lung tissue. The fact that we observed rapid formation of the cystic lesions and that they persisted, supports the hypothesis that FGF10 is involved in the early inductive events in CCAM formation and that continued presence of FGF10 is not necessarily required in the natural evolution of CCAM malformations.

Although speculative, our results can be interpreted in the context of current models of FGF10 involvement in branching

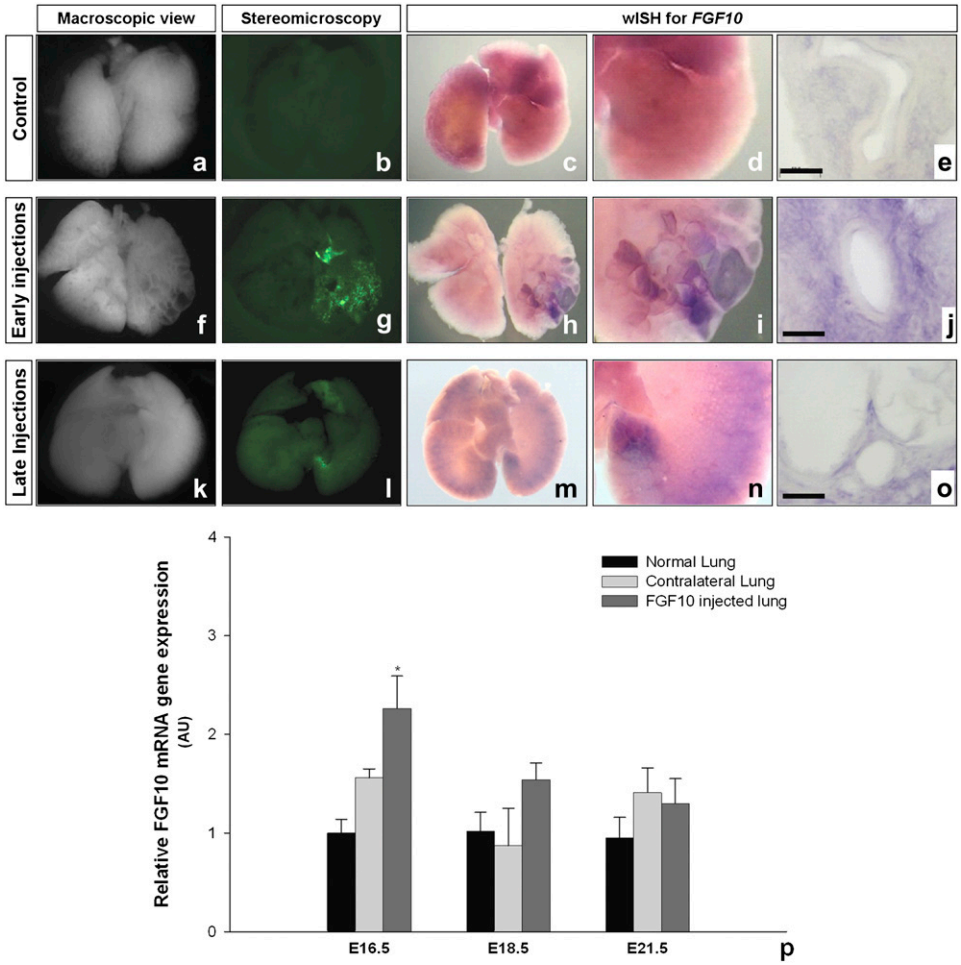

Figure 4. FGF10 mesenchymal overexpression coincides with location of cystic malformations. Lungs from injected fetuses at E15.5 and E18.5 were analyzed by whole mount *in situ* hybridization (wISH) for *fgf10*, 24 hours after injection (E16.5, *f–j*, and E19.5, *k–o*, respectively). The macroscopic view (*a*, *f*, *k*) and fluorescence stereomicroscopy images for GFP (*b*, *g*, *l*) are depicted alongside the wISH images for comparison. *FGF10* is overexpressed in the mesenchyme of the cystic area (*h–j*; *m–o*). (*p*) Quantitative PCR for *FGF10* in lung. *FGF10* expression of injected lungs at E15.5 was analyzed at E16.5, E18.5, and E21.5. Quantitative PCR was performed in PBS control, AdGFP-FGF10 injected, and contralateral lungs. *Fgf10* mRNA levels were significantly higher at E16.5 in AdGFP-FGF10 ipsilateral lungs versus PBS and contralateral lungs. However, at E18.5 and E21.5 *FGF10* expression was not significantly different among groups. *Scale bars* correspond to 50 μm for methacrylate sections of hybridized lungs.

morphogenesis (27) in which FGF10 and reciprocal influences such as Bmp4 and Spry2 regulate lung development (Figure 6). Under normal circumstances, cross-talk between the mesenchyme and the endodermal epithelium regulates the spatial and temporal gene expression for *fgf10*, *Bmp4*, and many other morphoregulatory molecules. Highly localized expression of *fgf10* in the mesenchyme adjacent to the tip of the nascent airway stimulates proliferation and growth outward. Simultaneously, FGF10 signaling induces a steady increase in *Bmp4* or other reciprocal factors transcription in epithelial cells. Bmp4 and Spry2 are inhibitory to epithelial cell proliferation/movement arresting the outward movement of the developing airway (8, 10). Branching is then induced by lateral up-regulation of mesenchymal FGF10 inducing dichotomous branching of the more proximal epithelium that remains responsive to FGF10. Thus during early stages of branching morphogenesis, high levels of mesenchymal FGF10 expression would be expected to induce a burst of proliferation and outward migration of the epithelium in segments of the developing airways between branch points that would be expected to be responsive to FGF10, with less proliferation at branch points where Bmp4 and other antagonists were expressed. While reciprocal signals such as Bmp4 would be expected to be diffusely induced in the epithelium, the ultimate size of the cyst would depend upon the balance of proliferative versus inhibitory signaling. *In situ* hybridization for BMP4 and for Spry2 indicated that their regulatory action over FGF10 might not be effective in lungs that were injected at earlier stages, because they are not concomitantly overexpressed. Thus, at the early time point, within the first 24 to 48 hours when FGF10 levels are high, one would

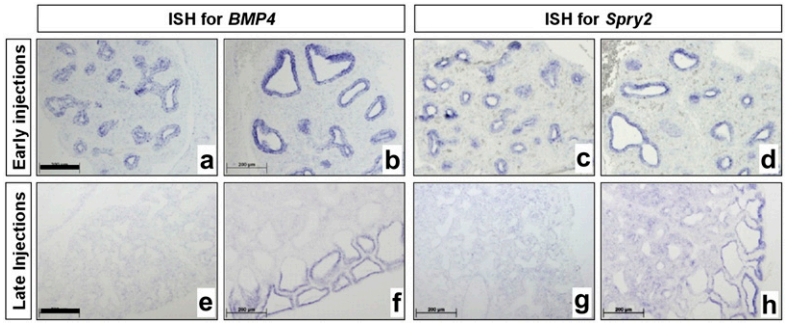

Figure 5. BMP4 and Spry2 expression pattern in cystic malformations. Lungs from injected fetuses at E15.5 and E18.5 were analyzed by *in situ* hybridization (ISH) for *bmp4 and spry2*, 24 hours after injection (E16.5, *a–d*; and E19.5, *e–h*, respectively). For AdGFP-FGF10 early injected lungs (*b*, *d*) the expression pattern of *BMP4* and *Spry2* does not seem altered in relation to respective controls (*a*, *c*). For AdGFP-FGF10 late injected lungs (*f*, *h*) expression of *BMP4* and *Spry2* is increased in the epithelium of the cystic malformations when compared with controls (*e*, *g*). *Scale bars* correspond to 200 μm.

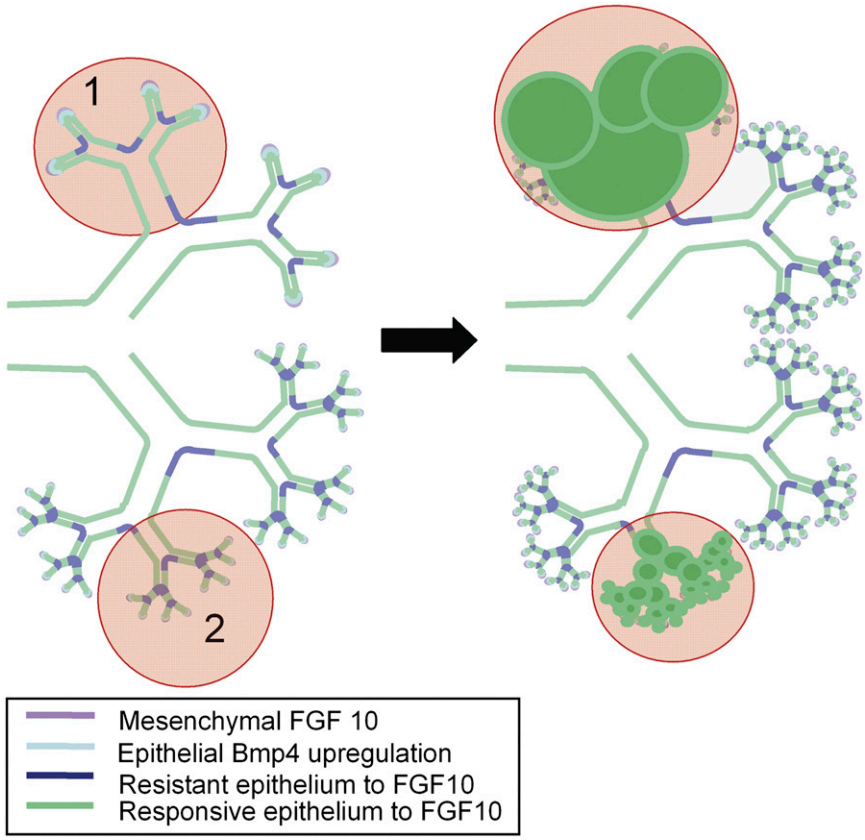

Figure 6. Model of FGF10 induction of cystic adenomatoid malformations. During the pseudoglandular and early canalicular phases the lung consists of repeating branch points with terminal growth determined by mesenchymal epithelial interaction orchestrated by mesenchymal FGF10 expressed at the tips of the elongating airways. By the model of Weaver and coworkers (10), FGF10 induces Bmp4 (or other FGF10 antagonists) in the adjacent epithelium, which renders the epithelium resistant to FGF10, stopping airway extension and creating a branch point with dichotomous branching induced by lateral FGF10 stimulation of the more proximal responsive airway epithelium. By this model, either proximal or early FGF10 overexpression as depicted by *pink circle 1* would stimulate a limited number of more proximal or less differentiated responsive airway segments, resulting in large cystic malformations. Whereas distal FGF10 overexpression as depicted by *circle 2* would stimulate a larger number of distal or more differentiated FGF10-responsive airway segments, respectively, resulting in a large number of smaller cysts. The cysts would tend to enlarge until induction of Bmp4 and other reciprocal factors resulted in epithelial inhibition or the FGF10 concentration diminished. The lining epithelium would be composed of the differentiated progeny of the lining epithelium of the proximal versus distal stimulated segment, that is, either bronchial or alveolar type epithelium, respectively. Although not shown in this cartoon, late FGF10 overexpression would be predicted to act on differentiated epithelium and terminally differentiated airways resulting in more adenomatous hyperplasia rather than cystic malformation.

expect unopposed action of FGF10 with rapid formation of large cysts. In contrast, in late injected lungs it was clear that expression of these two factors increase in the epithelium surrounding cystic areas. In this case, the significant induction of these regulatory molecules might be responsible for the inhibitory effect on FGF10-induced proliferation, leading to the formation of smaller cysts in late injected lungs. Also, in the proximal airways, where fewer branch points exist, and high columnar epithelium predominates, unopposed FGF10 signaling would be predicted to result in large cysts lined by predominantly bronchial epithelium. In distal airways, where multiple branch points are already present and cuboidal epithelium predominates, smaller and more numerous cysts would form lined by predominantly alveolar epithelium. In contrast, during the canalicular stage of lung development only terminal branching occurs and the distal airways are lined predominantly by cuboidal epithelium which is beginning to flatten and differentiate into type I and type II pneumocytes. Thus FGF10 overexpression might stimulate short segments of responsive epithelium into small cyst formation but the predominant effect would be expected to be similar to the effect of conditional FGF10 overexpression in postnatal lungs in which differentiated adenomas lined by abundant Type II epithelial cells form.

Ch'in and Tang identified CCAM as a pathologic entity in 1949 (27). While the pre- and postnatal natural history of CCAM is now well defined (28, 29), the pathogenesis of CCAM remains unknown. Diagnosis of CCAM in fetal life is usually made by ultrasound evaluation, and typically lesions are confined to a single lobe and can be classified as macrocystic or microcystic. In humans, macrocystic CCAMs have large cysts (2–10 cm) that vary in size and number with thin intervening echogenic areas. These multiple cysts are interconnected, and typically communicate with the tracheobronchial tree. The microcystic classification is applied to lesions that appear as a well delineated echogenic area in the fetal lung with no macrocystic spaces being identified. A CCAM categorization between the macrocystic and microcystic "definition" is sometimes used where the cyst spaces are present but small to moderate sized (< 2 cm) with adjacent echogenic tissue areas (30, 31). The ultrasound and MRI appearance, lobar distribution, and ultrasound classification of the malformations observed in this study were strikingly similar to human CCAM. FGF10 gene transfer during the pseudoglandular stage resulted in macrocystic lesions by ultrasound classification that were confirmed by MRI evaluation at Postnatal Day 7. A completely different ultrasound pattern was observed when gene transfer was performed during the canalicular stage—no cysts were visualized, but well-defined areas of increased echogenicity could be identified. MRI performed on microcystic lesions at 7 days after birth demonstrated very small cysts with careful analysis of images. The clinical manifestations of our induced lesions were also suggestive of human CCAM. CCAMs may grow rapidly before birth to massive size, resulting in extreme mediastinal shift and compromise of cardiac output resulting in fetal heart failure (hydrops); they may cause respiratory distress after birth; or they may be asymptomatic. It is not uncommon for CCAMs to undergo a rapid growth phase, only to decrease in size later in gestation. The same spectrum of clinical manifestations was observed in this study ranging from pre- or perinatal death from large, mass displacing tumors to asymptomatic survivors.

Stocker classified CCAMs into five subtypes defined on the basis of clinical features, macroscopic and microscopic criteria, and the site of the defect in the tracheobronchial tree (32). Depending on differences in cytodifferentiation, CCAM can be

divided into two major subtypes: CCAM types 1, 2, and 3, consisting of tissue with a bronchiolar-type epithelial differentiation; and a second subtype consisting of CCAM type 4, which has an acinar-alveolar epithelial differentiation. These two major subtypes have been hypothesized to originate at distinct stages of lung development: the first subtype (CCAM types 1, 2, and 3) may develop at the pseudoglandular stage, and the second subtype (CCAM type 4) may be due to a late event that disrupts branching of the distal acinar structures in the saccular period (33). Our study supports this pathophysiologic hypothesis. In this study we could reproduce the two histologic subtypes of CCAM. When proximal overexpression of FGF10 was induced during the pseudoglandular phase, we induced large cysts lined by tall to columnar epithelium with a high density of Clara cells and only few type II pneumocytes, resembling bronchiolar-type epithelial differentiation. Furthermore, when distal overexpression of FGF10 was induced during the canalicular phase, we observed small cysts composed of cuboidal epithelial that were primarily type II pneumocytes, resembling acinar epithelial differentiation.

There have been a number of efforts to characterize the molecular basis of CCAM in surgical specimens collected in both the pre- and postnatal periods. Cass and collaborators demonstrated that there is increased proliferation and decreased apoptosis in fetal CCAMs (34). *Fgf7* gene expression or protein production was evaluated in CCAMs requiring fetal resection, and no differences were found when compared with normal lungs (34). Platelet-derived growth factor-BB (PDGF-BB) gene expression and protein production were found to be increased in CCAMs that grew rapidly and required *in utero* resection (35), but there is no evidence that this factor is the causative factor for CCAM. Glial cell–derived neurotrophic factor (GDNF) was another factor with abnormal expression in epithelial cells lining CCAM cysts, suggesting a focal arrest in lung maturation during the fetal period (36). Although abnormal Hoxb-5 expression at a level typical of earlier lung developmental stages was observed in CCAM (37), it is presently unclear what initially triggers the cascade of events that ends with these malformations. All these studies have a common major limitation, which is that the analysis was performed in CCAM specimens that were surgically resected, analysis of which is unlikely to reveal the initial inciting events. In the present study, we have been able to evaluate in a prospective fashion the formation of CCAM-like malformations in response to overexpression of FGF10 in the mesenchymal compartment of the developing lung. We have demonstrated that transient overexpression of a single gene in a focal area of the lung is sufficient to reproduce the spectrum of gross and histologic features of human CCAM in a rat model. The striking similarity of these lesions to those seen in human CCAM strongly implicates mesenchymal overexpression of FGF10 in the initial events invoking CCAM formation. Our data thus far support FGF10 overexpression as the most important mechanistic component of CCAM formation. However, the identity of the primary mesenchymal perturbation that induces FGF10 overexpression remains to be determined.

Conflict of Interest Statement: None of the authors has a financial relationship with a commercial entity that has an interest in the subject of this manuscript.

Acknowledgments: The authors thank Dr. Suzanne Wehrli (Nuclear Magnetic Resonance Core Facility, The Joseph Stokes Jr. Research Institute, Philadelphia, PA) for the magnetic resonance imaging, and Antoneta Radu and Lauren Robinson for their invaluable technical assistance in this study.

References

1. Perl AK, Whitsett JA. Molecular mechanisms controlling lung morphogenesis. *Clin Genet* 1999;56:14–27.
2. Warburton D, Schwarz M, Tefft D, Flores-Delgado G, Anderson KD, Cardoso WV. The molecular basis of lung morphogenesis. *Mech Dev* 2000;92:55–81.
3. Post M, Souza P, Liu J, Tseu I, Wang J, Kuliszewski M, Tanswell AK. Keratinocyte growth factor and its receptor are involved in regulating early lung branching. *Development* 1996;122:3107–3115.
4. Ulich TR, Yi ES, Longmuir K, Yin S, Biltz R, Morris CF, Housley RM, Pierce GF. Keratinocyte growth factor is a growth factor for type II pneumocytes in vivo. *J Clin Invest* 1994;93:1298–1306.
5. Bellusci S, Grindley J, Emoto H, Itoh N, Hogan BL. Fibroblast growth factor 10 (fgf10) and branching morphogenesis in the embryonic mouse lung. *Development* 1997;124:4867–4878.
6. De Moerlooze L, Spencer-Dene B, Revest J, Hajihosseini M, Rosewell I, Dickson C. An important role for the IIIb isoform of fibroblast growth factor receptor 2 (FGFR2) in mesenchymal-epithelial signalling during mouse organogenesis. *Development* 2000;127:483–492.
7. Peters KG, Werner S, Chen G, Williams LT. Two FGF receptor genes are differentially expressed in epithelial and mesenchymal tissues during limb formation and organogenesis in the mouse. *Development* 1992;114:233–243.
8. Mailleux AA, Tefft D, Ndiaye D, Itoh N, Thiery JP, Warburton D, Bellusci S. Evidence that SPROUTY2 functions as an inhibitor of mouse embryonic lung growth and morphogenesis. *Mech Dev* 2001; 102:81–94.
9. Tefft JD, Lee M, Smith S, Leinwand M, Zhao J, Bringas P Jr, Crowe DL, Warburton D. Conserved function of mSpry-2, a murine homolog of Drosophila sprouty, which negatively modulates respiratory organogenesis. *Curr Biol* 1999;9:219–222.
10. Weaver M, Dunn NR, Hogan BL. Bmp4 and Fgf10 play opposing roles during lung bud morphogenesis. *Development* 2000;127:2695–2704.
11. Eblaghie MC, Reedy M, Oliver T, Mishina Y, Hogan BL. Evidence that autocrine signaling through Bmpr1a regulates the proliferation, survival and morphogenetic behavior of distal lung epithelial cells. *Dev Biol* 2006;291:67–82.
12. Cardoso WV, Lu J. Regulation of early lung morphogenesis: questions, facts and controversies. *Development* 2006;133:1611–1624.
13. Sekine K, Ohuchi H, Fujiwara M, Yamasaki M, Yoshizawa T, Sato T, Yagishita N, Matsui D, Koga Y, Itoh N, *et al.* FGF10 is essential for limb and lung formation. *Nat Genet* 1999;21:138–141.
14. Guo L, Degenstein L, Fuchs E. Keratinocyte growth factor is required for hair development but not for wound healing. *Genes Dev* 1996;10: 165–175.
15. Simonet WS, DeRose ML, Bucay N, Nguyen HQ, Wert SE, Zhou L, Ulich TR, Thomason A, Danilenko DM, Whitsett JA. Pulmonary malformation in transgenic mice expressing human keratinocyte growth factor in the lung. *Proc Natl Acad Sci USA* 1995;92:12461–12465.
16. Clark JC, Tichelaar JW, Wert SE, Itoh N, Perl AK, Stahlman MT, Whitsett JA. Fgf-10 disrupts lung morphogenesis and causes pulmonary adenomas in vivo. *Am J Physiol Lung Cell Mol Physiol* 2001;280: L705–L715.
17. Panos RJ, Rubin JS, Csaky KG, Aaronson SA, Mason RJ. Keratinocyte growth factor and hepatocyte growth factor/scatter factor are heparin-binding growth factors for alveolar type II cells in fibroblast-conditioned medium. *J Clin Invest* 1993;92:969–977.
18. Park WY, Miranda B, Lebeche D, Hashimoto G, Cardoso WV. FGF-10 is a chemotactic factor for distal epithelial buds during lung development. *Dev Biol* 1998;201:125–134.
19. Sutherland D, Samakovlis C, Krasnow MA. Branchless encodes a drosophila fgf homolog that controls tracheal cell migration and the pattern of branching. *Cell* 1996;87:1091–1101.
20. Henriques-Coelho T, Gonzaga S, Endo M, Zoltick PW, Davey M, Leite-Moreira AF, Correia-Pinto J, Flake AW. Targeted gene transfer to fetal rat lung interstitium by ultrasound-guided intrapulmonary injection. *Mol Ther* 2007;15:340–347.
21. He TC, Zhou S, da Costa LT, Yu J, Kinzler KW, Vogelstein B. A simplified system for generating recombinant adenoviruses. *Proc Natl Acad Sci USA* 1998;95:2509–2514.
22. Henrique D, Adam J, Myat A, Chitnis A, Lewis J, Ish-Horowicz D. Expression of a delta homologue in prospective neurons in the chick. *Nature* 1995;375:787–790.
23. Strahle U, Blader P, Adam J, Ingham PW. A simple and efficient procedure for non-isotopic in situ hybridization to sectioned material. *Trends Genet* 1994;10:75–76.
24. Chomczynski P, Sacchi N. Single-step method of RNA isolation by acid guanidinium thiocyanate-phenol-chloroform extraction. *Anal Biochem* 1987;162:156–159.

25. Gilliland G, Perrin S, Blanchard K, Bunn HF. Analysis of cytokine mRNA and DNA: detection and quantitation by competitive polymerase chain reaction. *Proc Natl Acad Sci USA* 1990;87:2725–2729.
26. Sambrook J, Fritch EF, Maniatis T. Molecular cloning: a laboratory manual. Cold Spring Harbor, NY: Cold Spring Harbor Laboratory Press; 1989.
27. Ch'in KT, Tang MY. Congenitalcystic adenomatoid malformation of one lobe of lung with general anasarca. *Arch Pathol (Chic)* 1949;48: 221–229.
28. Adzick NS. Fetal cystic adenomatoid malformation of the lung: diagnosis, perinatal management, and outcome. *Semin Thorac Cardiovasc Surg* 1994;6:247–252.
29. Adzick NS, Harrison MR, Glick PL, Golbus MS, Anderson RL, Mahony BS, Callen PW, Hirsch JH, Luthy DA, Filly RA, *et al.* Fetal cystic adenomatoid malformation: prenatal diagnosis and natural history. *J Pediatr Surg* 1985;20:483–488.
30. Adzick NS, Harrison MR, Crombleholme TM, Flake AW, Howell LJ. Fetal lung lesions: management and outcome. *Am J Obstet Gynecol* 1998;179:884–889.
31. Wilson RD, Hedrick HL, Liechty KW, Flake AW, Johnson MP, Bebbington M, Adzick NS. Cystic adenomatoid malformation of the lung: review of genetics, prenatal diagnosis, and in utero treatment. *Am J Med Genet A* 2006;140:151–155.
32. Stocker JT. Congenital and developmental diseases. In: Dail DH, Hammer SP, editors. Pulmonary pathology. New York, NY: Springer; 1994. pp. 174–180.
33. Morotti RA, Cangiarella J, Gutierrez MC, Jagirdar J, Askin F, Singh G, Profitt SA, Wert SE, Whitsett JA, Greco MA. Congenital cystic adenomatoid malformation of the lung (ccam): evaluation of the cellular components. *Hum Pathol* 1999;30:618–625.
34. Cass DL, Quinn TM, Yang EY, Liechty KW, Crombleholme TM, Flake AW, Adzick NS. Increased cell proliferation and decreased apoptosis characterize congenital cystic adenomatoid malformation of the lung. *J Pediatr Surg* 1998;33:1043–1046. (discussion 1047).
35. Liechty KW, Crombleholme TM, Quinn TM, Cass DL, Flake AW, Adzick NS. Elevated platelet-derived growth factor-b in congenital cystic adenomatoid malformations requiring fetal resection. *J Pediatr Surg* 1999;34:805–809. (discussion 809–810).
36. Fromont-Hankard G, Philippe-Chomette P, Delezoide AL, Nessmann C, Aigrain Y, Peuchmaur M. Glial cell-derived neurotrophic factor expression in normal human lung and congenital cystic adenomatoid malformation. *Arch Pathol Lab Med* 2002;126:432–436.
37. Volpe MV, Martin A, Vosatka RJ, Mazzoni CL, Nielsen HC. Hoxb-5 expression in the developing mouse lung suggests a role in branching morphogenesis and epithelial cell fate. *Histochem Cell Biol* 1997;108: 495–504.